

Corrosion–Fatigue Fracture of the Ultrafine-Grained PT-7M Titanium Alloy Fabricated by Rotary Forging

V. N. Chuvil'deev^a, N. N. Berendeev^a, A. A. Murashov^a, V. I. Kopylov^{a, b}, A. V. Nokhrin^{a, *},
M. Yu. Gryaznov^a, K. V. Likhmitskii^a, N. Yu. Tabachkova^c, E. A. Galaeva^a, D. N. Kotkov^a,
A. M. Bakhmet'ev^d, T. V. Tryaev^d, and M. M. Myshlyaev^e

^aNizhny Novgorod State University, Nizhny Novgorod, 603600 Russia

^bPhysicotechnical Institute, Belarussian Academy of Sciences, Minsk, 220141 Belarus

^cNational University of Science and Technology MISiS, Moscow, 119049 Russia

^dAO Afrikantov OKB Mechanical Engineering Company, Nizhny Novgorod, 603074 Russia

^eBaikov Institute of Metallurgy and Materials Science, Russian Academy of Sciences, Moscow, 119991 Russia

*e-mail: nokhrin@nifti.unn.ru

Received February 12, 2019; revised November 20, 2019; accepted December 5, 2019

Abstract—The corrosion–fatigue fracture of an ultrafine-grained Ti–2.2Al–2.5Zr pseudo- α titanium alloy (PT-7M alloy), which is used in atomic power engineering, is studied. The formation of an ultrafine-grained structure by rotary forging is found to increase the corrosion–fatigue strength. The parameters in Basquin's equation are determined, and the slope of the σ_a – $\log N$ fatigue curve is shown to nonmonotonically depend on the temperature of annealing of the ultrafine-grained alloy.

Keywords: titanium alloy, ultrafine-grained structure, rotary forging, corrosion fatigue

DOI: 10.1134/S0036029520070058

INTRODUCTION

Titanium alloys are widely used in atomic power engineering to produce the heat-exchange equipment of nuclear power plants (NPPs) [1]. The titanium alloys used for NPPs must meet high strength, plasticity, corrosion resistance, and radiation resistance requirements [1, 2]. For this purpose, researchers use various methods of forming an ultrafine-grained (UFG) structure by severe plastic deformation (SPD) methods [3–10].

One of the most dangerous degradation processes in the heat-exchange equipment of NPP is corrosion–fatigue fracture, which often occurs at high temperatures during hot salt corrosion [2, 11]. Despite deep interest in studying corrosion–fatigue fracture [12, 13], its mechanisms in high-strength UFG titanium alloys are still poorly understood, which complicates the prediction of the behavior of NPP heat exchangers.

In particular, the causes of the weak influence of corrosive media on the fatigue strength characteristics of titanium alloys are still poorly understood: as was shown in [1, 14, 15], the fatigue fracture curves σ_a – $\log N$ (σ_a is the applied stress amplitude, N is the number of cycles to failure) of smooth specimens of α and pseudo- α alloys almost coincide with each other on testing in air and neutral (weakly acid) aqueous media, and tests with preliminarily formed fatigue cracks demonstrate a high sensitivity of titanium alloys to the presence of a corrosive media [1]. As was shown in [16, 17], the fatigue strength characteristics of two-

phase titanium alloys (VT6, VT14, etc.) decrease in the presence of a neutral medium, and the fatigue limit of α and pseudo- α alloys (PT-3V, PT-7M) increases insignificantly during tests in a 3% aqueous solution of NaCl as compared to fatigue tests in air. The available data on the contribution of microplastic deformation to the fatigue fracture of high-plasticity titanium alloys and on the influence of the grain size and the structure–phase state of grain boundaries on the rate of corrosion–fatigue fracture of titanium alloys are also conflicting.

The purpose of this work is to study the corrosion–fatigue fracture of a high-strength UFG PT-7M α titanium alloy.

EXPERIMENTAL

We studied a commercial PT-7M pseudo- α titanium alloy of the composition Ti–2.5% Al–2.6% Zr.¹ The chemical composition of the alloy met the requirements of GOST 19807–91. Forgings of the coarse-grained (CG) PT-7M alloy were fabricated at AO Chepetsk engineering works (Glazov) under standard thermomechanical treatment conditions.

An UFG structure was formed during deformation of a rod 20 mm in diameter into a rod 6 mm in diameter by rotary forging (RF) on an R5-4-21 HMP (Germany) RF machine at room temperature. The total

¹ Hereafter, the element contents are given in wt %.

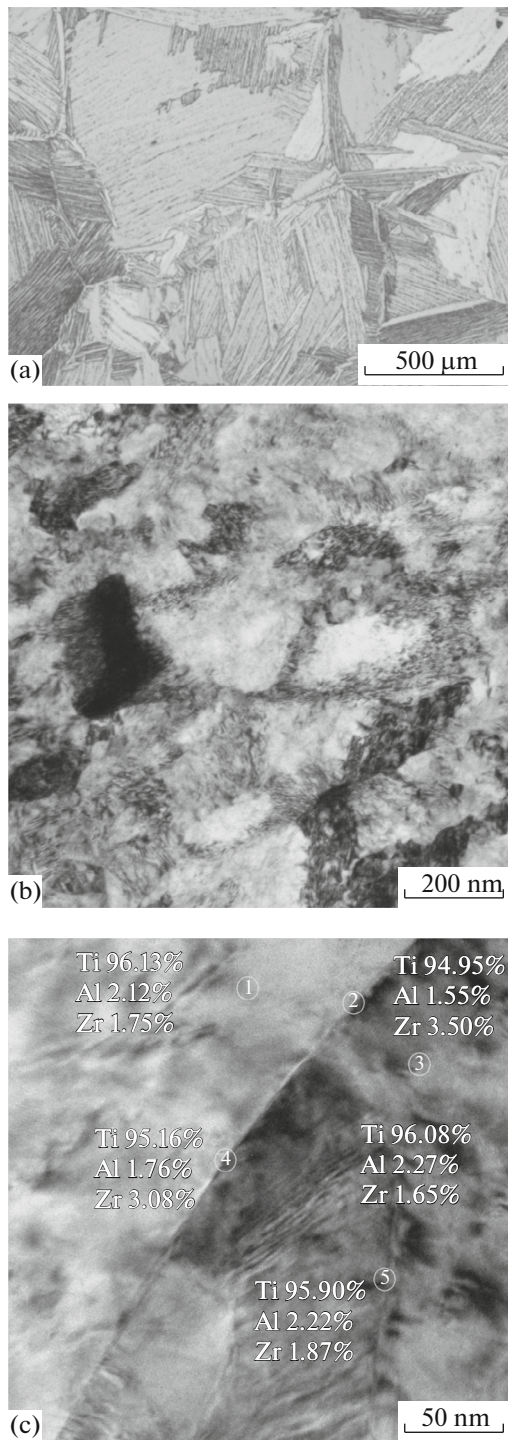


Fig. 1. Microstructure of the PT-7M alloy: (a) initial CG state, (b) UFG state after RF, and (c) data of local energy dispersive microanalysis (points 1–5) of grain boundaries and the near-boundary regions in the UFG alloy.

cumulative strain was $\varepsilon = 70\%$ and the strain rate was $\dot{\varepsilon} = 0.5\text{--}1\text{ s}^{-1}$.

X-ray diffraction (XRD) analysis was carried out with a DRON-3 diffractometer. A structure was analyzed using a Leica IM DRM optical microscope, a

JEOL JSM6490 scanning electron microscope equipped with an Oxford Instruments INCA 350 energy dispersive microanalyzer, and a JEOL JEM2100 transmission electron microscope equipped with a JED-2300 energy dispersive microanalyzer. To reveal a microstructure, we subjected metallographic sections to mechanical polishing and electrolytic etching in the solution $75\% \text{H}_2\text{SO}_4 + 15\% \text{HNO}_3 + 10\% \text{HF}$ at room temperature. The macrostructure of the rod was revealed by etching in the aqueous solution $15\% \text{HF} + 10\% \text{HNO}_3 + 35\% \text{glycerol}$. Foils for transmission electron microscopy (TEM) examination were spark-cut across the rod axis and were then mechanically and electrolytically thinned.

Internal stresses σ_{int} were studied by an XRD method and were calculated by the Williamson–Hall method [18]. Before an investigation, the sample surface was subjected to mechanical polishing to a roughness level $R_z < 1\ \mu\text{m}$ and subsequent electrochemical polishing to remove a cold-worked layer.

Room-temperature tensile tests were carried out on smooth flat specimens with a 3-mm-thick gage portion (specimen 23, type I according to GOST 1497–85) and on cylindrical specimens with a gage portion 3 mm in diameter (specimen 9, type III according to GOST 1497–85). Microhardness was measured on an HVS-1000 hardness tester at a load of 2 N (200 gf).

The corrosion–fatigue tests of smooth cylindrical specimens with a gage portion 3 mm in diameter (type II according to GOST 25.502–79) were performed in a 3% aqueous solution of NaCl according to the cantilevered bending scheme (stress ratio was $R_\sigma = -1$) at a frequency of 50 Hz. The roughness of the gage portion in the specimens was $R_z = 3.2\ \mu\text{m}$. Fractographic analysis of the fracture surfaces of the specimens subjected to corrosion–fatigue tests was carried out on the JEOL JSM6490 scanning electron microscope. Before fractographic analysis, the fracture surfaces were subjected to ultrasonic cleaning. Fatigue curves were analyzed using Basquin's power equation $\sigma_a = AN^{-q}$, where A and q are numerical coefficients [19].

Specimens were annealed for 30 min in a SNOL air function and were then cooled in still air. The temperature was maintained accurate to $\pm 5^\circ\text{C}$. The oxygen content in the alloy after annealing met the requirements of GOST 19807–91. Annealing was performed to vary the structure–phase state of the UFG alloy, namely, to change the grain size and to relieve the internal stresses that formed during RF.

RESULTS AND DISCUSSION

In the initial (as-delivered) state, the PT-7M alloy has a conventional CG lamellar–acicular structure with stitch β -phase precipitates along titanium α' -phase boundaries (Fig. 1a). The α' -phase lamella thickness in the initial state is 5–10 μm and the lamella length is a few hundred microns. After RF, an UFG structure with an average fragment size of 0.2–0.5 μm

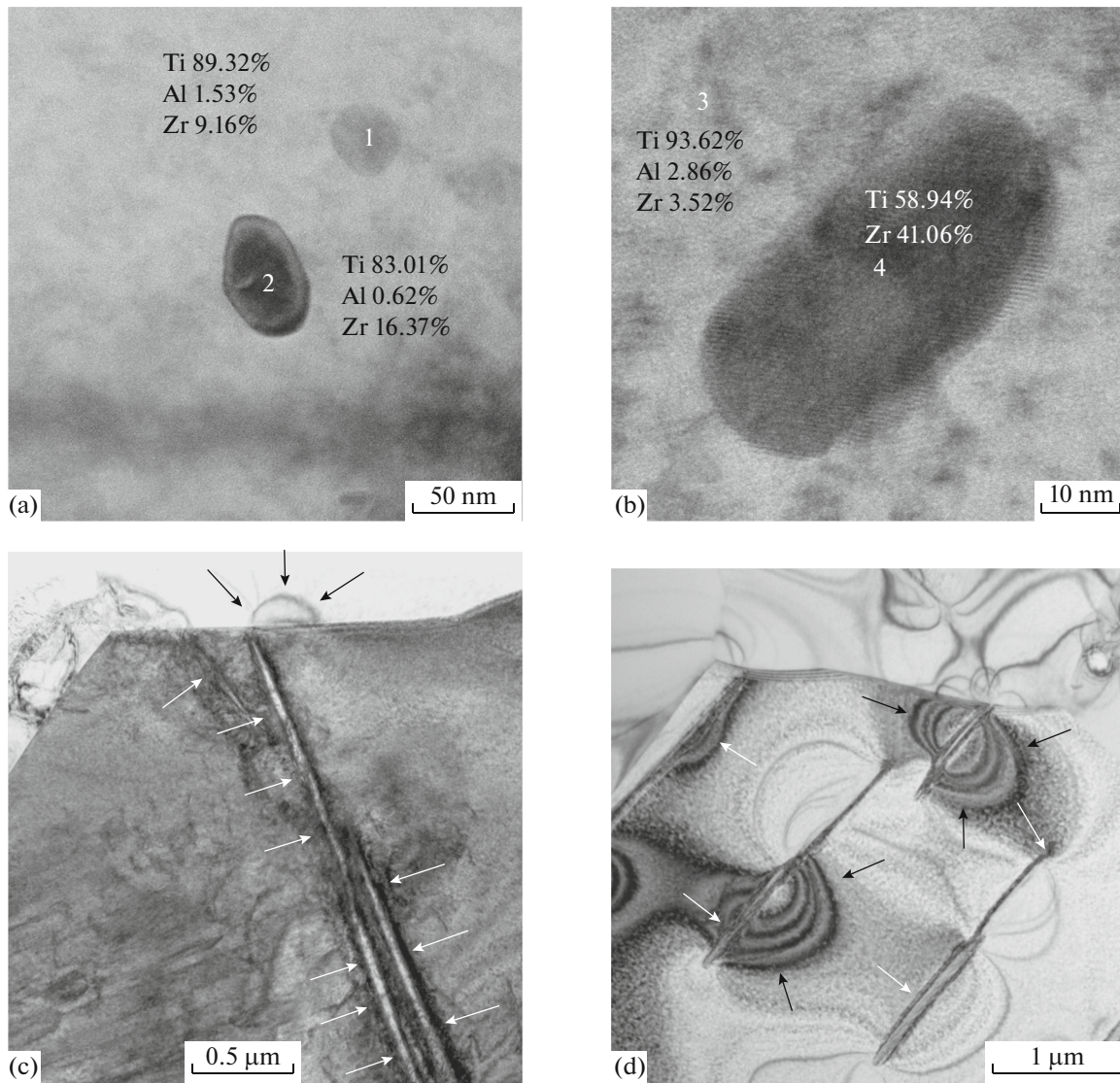


Fig. 2. Microstructure of the PT-7M alloy after RF and annealing ((a, b) zirconium particles in the alloy after annealing at 400 and 600°C, respectively) and the results of studying the composition of zirconium particles by energy dispersive analysis ((c, d) α' -phase particles are indicated by white arrows) in recrystallized α -Ti grains after annealing at 600 and 700°C, respectively; stress fields at interphase boundaries (at the sites where β -phase particles reach α -phase boundaries) are indicated by black arrows.

forms (Fig. 1b). An analysis of the electron-microscopic results demonstrates that the UFG structure after RF is a mixed grain–subgrain structure (see Fig. 1b). The results of local energy dispersive microanalysis of the UFG alloy show a high zirconium content and a low aluminum content along grain boundaries as compared to the near-boundary regions (Fig. 1c).

Annealing of the UFG PT-7M alloy at 400°C causes the precipitation of zirconium particles and the beginning of recovery, which is accompanied by a decrease in the lattice dislocation density with increasing annealing temperature. The zirconium particle sizes are 20–50 nm (Figs. 2a, 2b). Structural examination demonstrates that recrystallization and simulta-

neous dissolution of zirconium particles begin in the UFG titanium alloy after annealing at 500–550°C. After annealing at 650°C, the average grain size changes from 2.8–3.0 μm (surface layer) to 3.5–4.0 μm (central zone of the rod).

Electron-microscopic investigations show that lamellar second-phase (presumably, α' phase) particles form in the volume of recrystallized grains in the titanium alloy (Figs. 2c, 2d, 3). Local internal stress fields form at α/α' interphase boundaries (indicated by the black arrows in Figs. 2c, 2d). After annealing at 600–700°C, the lattice dislocation density is very low and zirconium particles in the structure of the recrystallized alloy are not detected.

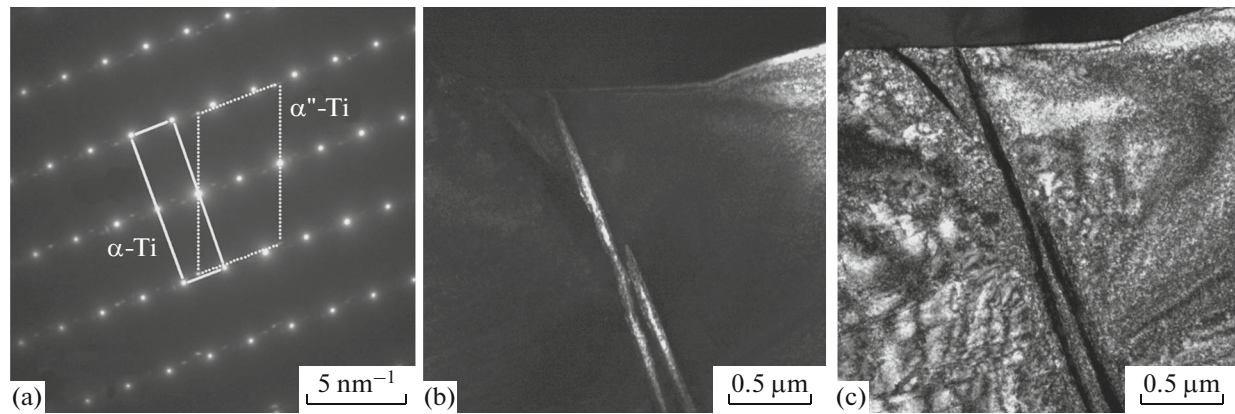


Fig. 3. (a) Electron diffraction pattern obtained on TEM analysis of α'' -phase particles in recrystallized α -Ti grains after annealing at 500°C and dark-field images of the particles taken with reflections of (b) α phase and (c) α'' phase.

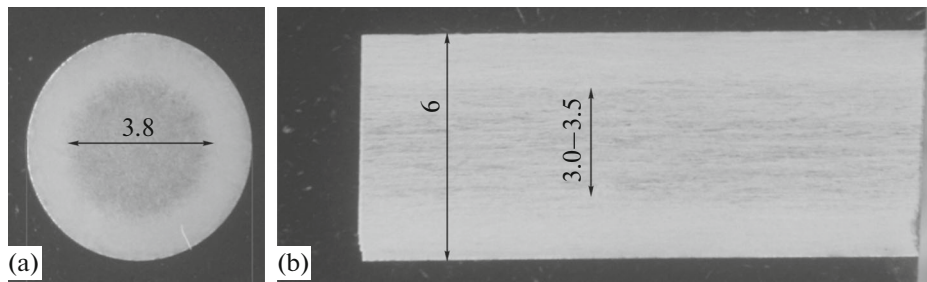


Fig. 4. Microstructures of (a) cross section and (b) longitudinal section of the PT-7M titanium alloy specimens after RF and recrystallization annealing at 650°C for 30 min.

Tensile tests demonstrate that the formation of an UFG structure leads to an increase yield strength $\sigma_{0.2}$ and ultimate tensile strength σ_u from 280 to 1050–1070 MPa and from 590 to 1080 MPa. The relative elongation decreases from 30–40 to 6–7%. The strain is nonuniformly distributed over the cross section of the rod in the state after RF: the hardness of the UFG alloy in the cross section decreases from 2.9–3.0 to 2.5–2.6 GPa when going from the periphery to the center. The heterogeneous granular structure in the recrystallized specimen is clearly visible on a polished macrosection as the strongly etched zone in the UFG structure in the central part of the rod (Fig. 4). For a further analysis, we note that a heterogeneous structure with different grain sizes, which is characteristic of the stage of primary recrystallization, forms at the initial stage of recrystallization annealing in the UFG PT-7M titanium alloy (Figs. 5a, 5b). The driving force of the primary recrystallization that occurs on annealing of severely deformed metals is known to be a decrease in the stored internal energy related to a high lattice dislocation density [20]. As a result, rapidly moving grain boundaries can “absorb” lattice dislocations and the related low-angle boundaries [21]. Note also that the average recrystallized-grain size in the surface layer of the PT-7M titanium alloy rod turns

out to be smaller than that in the central part of the cross section of the rod by 0.5–1 μm (Figs. 5c, 5d).

After annealing at 700°C for 30 min, the difference between the hardnesses of the central and surface zones in the cross section of the rod does not exceed 0.1–0.15 GPa. The mechanical properties of the annealed PT-7M alloy are as follows: $\sigma_{0.2} = 350$ –370 MPa, $\sigma_u = 600$ –620 MPa, and $\delta_5 = 12$ –14%. Figure 6a shows the stress σ –strain ϵ curves obtained for the UFG PT-7M alloy specimens annealed under various conditions and the dependences of yield strength $\sigma_{0.2}$, ultimate tensile strength σ_u , and relative elongation to failure δ on the annealing temperature (Fig. 6b).

The XRD study of the internal stresses showed that the formation of an UFG structure in the PT-7M titanium alloy caused tensile stresses: the level of internal stresses increased from $\sigma_{\text{int}} = 160 \pm 20$ to 520 ± 40 MPa.² After annealing at 700°C, we have $\sigma_{\text{int}} = 170 \pm 20$ MPa. Therefore, we can state that one of the causes

² The sign of internal stresses was determined from the shift in the position of the (100) peak of α -Ti according to the Wulff–Bragg equation $2d_{hk} \sin \theta_{\text{max}} = n\lambda$, where θ_{max} is the diffraction angle corresponding to the position of the (100) peak of α -Ti and λ is the X-ray wavelength ($\lambda = 1.54178 \text{ \AA}$).

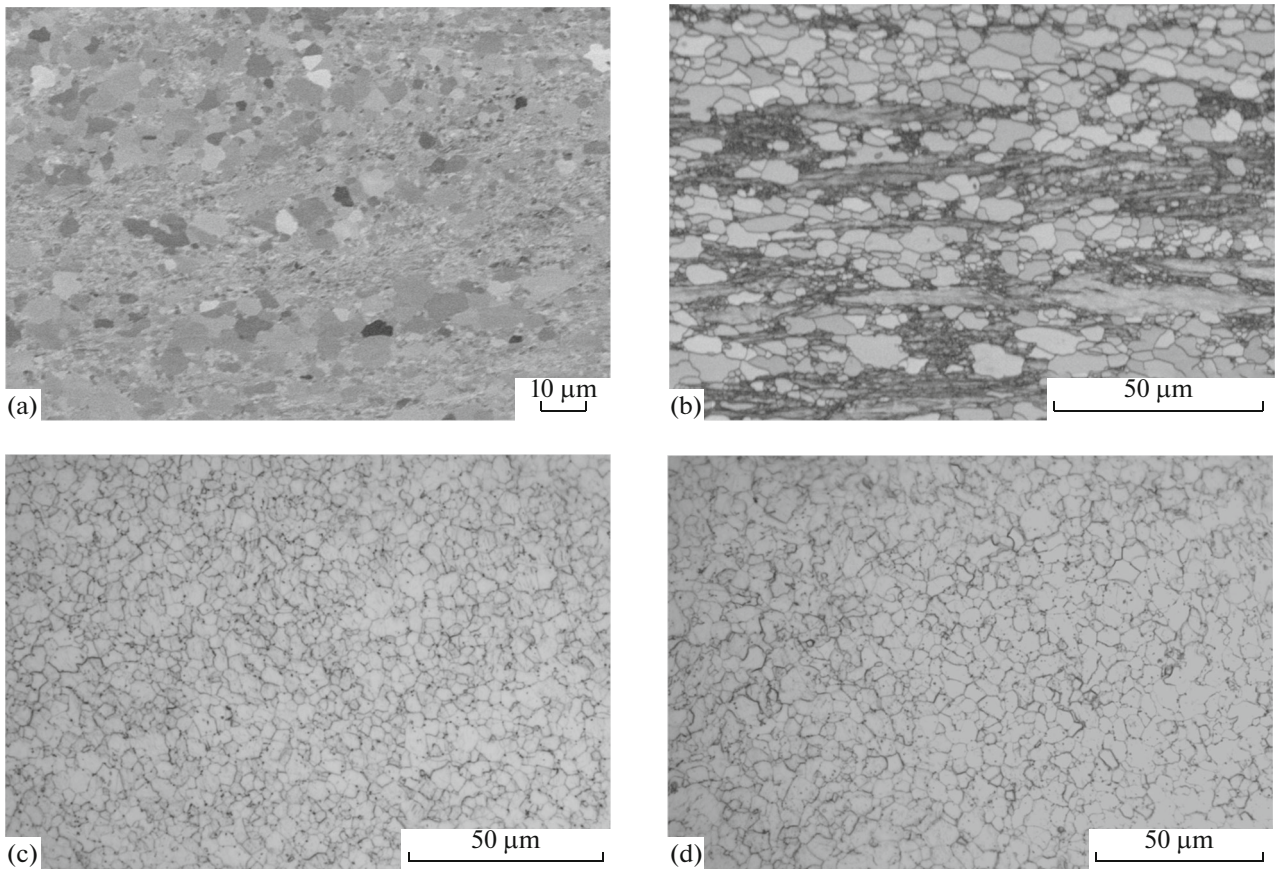


Fig. 5. Microstructures of (a, c) surface and (b, d) central layers of the PT-7M titanium alloy rod subjected to RF and annealing at (a, b) 600 and (c, d) 650°C.

of the low plasticity of the UFG PT-7M alloy after RF is represented by internal tensile stress fields.

Figure 7a shows the σ_a – N fatigue curves for the alloy in the CG and UFG states. The fatigue limit at $N^* = 3 \times 10^6$ cycles is $\sigma_{-1} = 320$ – 330 MPa for the CG alloy and $\sigma_{-1} = 570$ – 590 MPa for the UFG alloy after RF. σ_{-1} of the UFG alloy after annealing at 650°C decreases to ~ 500 MPa. Note that UFG structure formation leads to an increase in the life of the alloy at an amplitude $\sigma_a = 600$ MPa from $N_{fr} = 10^3$ to 4×10^4 – 5×10^5 cycles. It is important that this increase in the fatigue strength of the UFG alloy takes place at its low plasticity (relative elongation to failure decreases from 30–40% in the CG alloy to 6–7% in the UFG alloy). An increase in the annealing temperature from 500 to 650°C at $\sigma_a = 600$ MPa causes a decrease in N_{fr} from 7×10^5 to 1.5×10^5 loading cycles. After annealing at 650°C, the conventional fatigue limit is $\sigma_{-1} \approx 500$ MPa.

The large scatter of the data obtained for the UFG PT-7M alloy as compared to the CG alloy specimens is noteworthy (Fig. 7a). This scatter is thought to be related to a nonuniform strain distribution over the cross section of the rod (see Fig. 4). This assumption is

indirectly supported by the decrease in the scatter of the experimental points in the σ_a – N dependence during an increase in the temperature of annealing of the UFG PT-7M alloy, which leads to the formation of a homogeneous granular structure (see Fig. 7b).

Figures 8 and 9 show the results of fractographic examination of the fracture surfaces of the UFG PT-7M alloy. The fracture of the PT-7M alloy at a high solidification amplitude is seen to be mainly brittle: the fracture surfaces have numerous intragranular cleavage facets, traces of intragranular fracture along crystallographic planes located near a fatigue crack zone (CPs in Fig. 9), and traces of crack growth in coarse grains. Fatigue beachmark (FB) zones are visible in some favorably oriented elongated grains, and the average FB–FB distance is ~ 1 μm (Fig. 9). A final fracture zone can hardly be detected in the fracture surfaces of the CG PT-7M alloy, since its area is small at all stress amplitudes under study.

Fractographic analysis revealed one or several (depending on the applied amplitude) microcrack nucleation zones (zone ZI), a stable crack growth zone (ZIIa), an accelerated crack growth zone (ZIIb), and a final fracture zone (zone ZIII) in the fracture surfaces of the UFG PT-7M alloy (Figs. 10, 11). The final

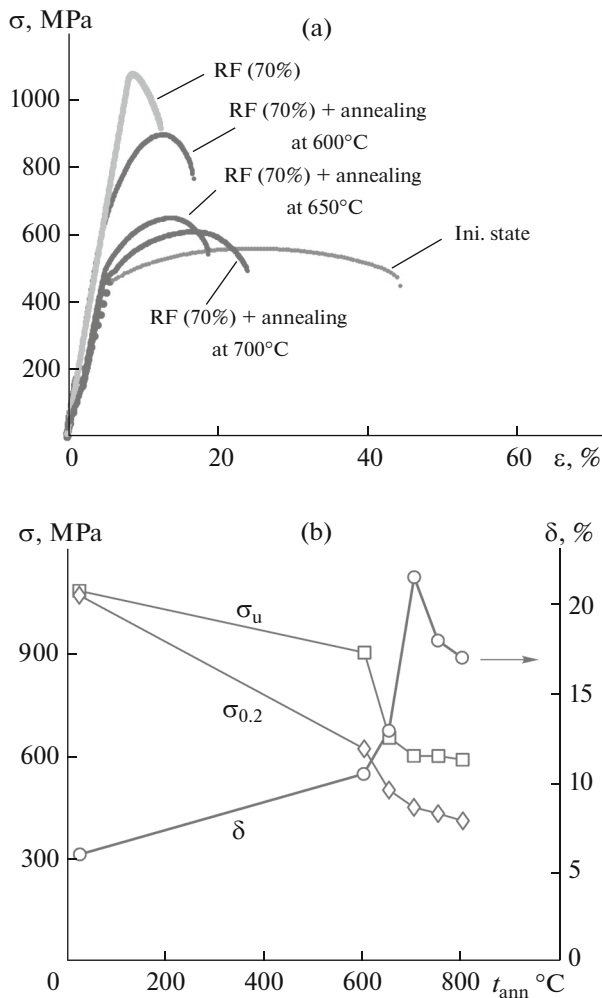


Fig. 6. Effect of annealing on the mechanical properties of the UFG PT-7M alloy: (a) stress–strain curves (Ini. state stands for the initial CG state of the alloy) and (b) mechanical properties of the UFG alloy vs. the temperature of 30-min annealing.

fracture zone area increases with σ_a and becomes comparable with the zone ZII area at $\sigma_a > 700$ MPa. An analysis of these results demonstrates that the fracture of the UFG alloy at the stage of stable crack growth has a mixed ductile–brittle character, and conventional intragranular cleavage facets are not observed in zone ZII because of a small grain size (see Fig. 11 and the classification in handbook [22]). The stable crack growth zone transforms gradually into the accelerated crack growth zone, which has secondary cracks. This finding indicates a high crack velocity, which is likely to be due to a high stress intensity factor. According to [22], the presence of secondary cracks points to a ductile character of fracture in the accelerated crack growth zone. Zone ZIII is characterized by a ductile type of fracture and has numerous dimples formed upon micropore coalescence (see Fig. 11). Note that the stable crack growth zone does not exceed

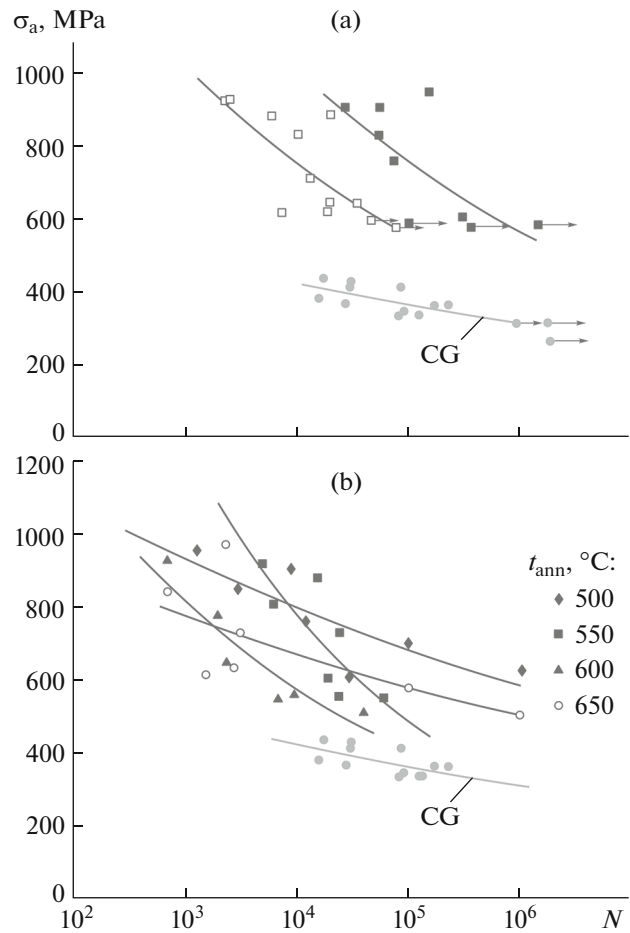


Fig. 7. Corrosion–fatigue curves for PT-7M alloy: (a) in the initial CG state and after RF in the UFG state (Basquin’s equation parameters are $A = 2805$ MPa, $q = 0.15$ (right branch) and $A = 3245$ MPa, $q = 0.12$ (left branch)) and (b) in the initial CG state and in the UFG state after annealing at various temperatures.

40% of the fracture surface area at all stress amplitudes. This value is significantly smaller than that in the CG alloy.

An analysis of the results of fractographic investigations demonstrates that an increase in the annealing temperature to 650°C (at a given stress amplitude) is accompanied by an increase in the number of microcrack nucleation zones, a decrease in the area occupied by the stable crack growth zone from 40–45 to 25–30%, and an increase in the fracture surface area corresponding to the accelerated crack growth zone from 30–35 to 55%. Figure 12 shows the results of fractographic analysis of the fracture surfaces. The final fracture zone area decreases slightly upon annealing from 25–30 to 15–20%. Figure 13 presents the results of fractographic analysis of some regions in the fracture surfaces of the UFG alloy subjected to annealing at 650°C. A comparison of the fracture surfaces of the CG and UFG specimens demonstrates that the

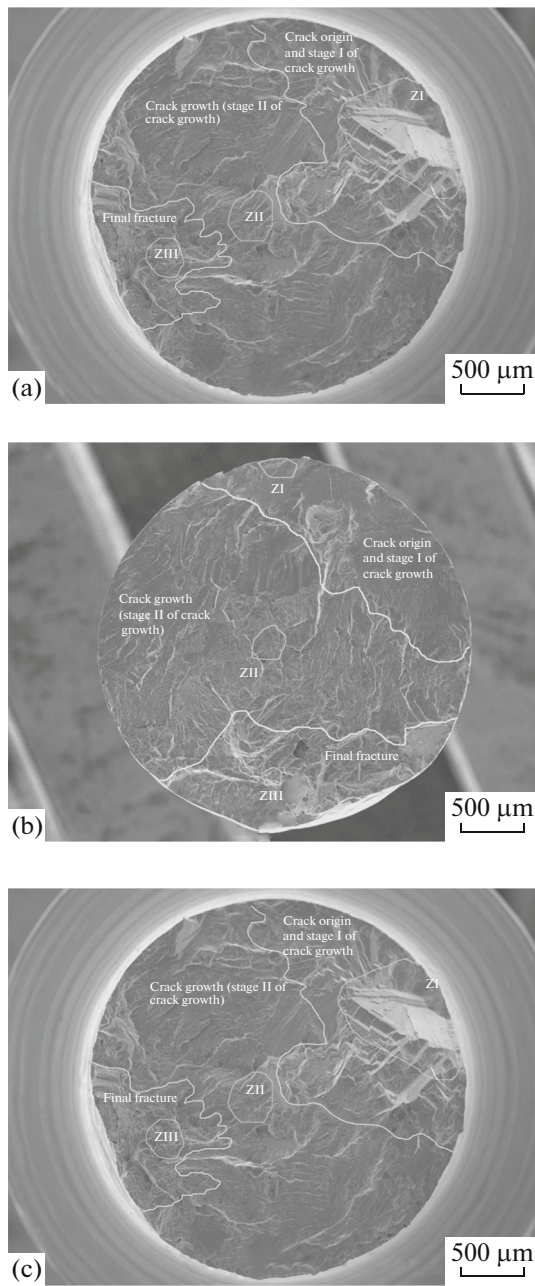


Fig. 8. Fractographic analysis of the fracture surfaces of the CG PT-7M alloy after corrosion–fatigue tests at a stress amplitude of (a) 335, (b) 380, and (c) 415 MPa. ZI, ZII, and ZIII are the crack origin, stable crack growth, and final fracture zones, respectively.

FB–FB distance in the CG specimens is much larger than that in the UFG specimens: at the same magnification, the FB–FB distance in the UFG specimens cannot be resolved, including fractographic analysis of the fracture surfaces of the UFG alloy specimens after recrystallization annealing. According to [22], this result is thought to indirectly indicate that the crack velocity in UFG alloys is much lower than that in CG alloys.

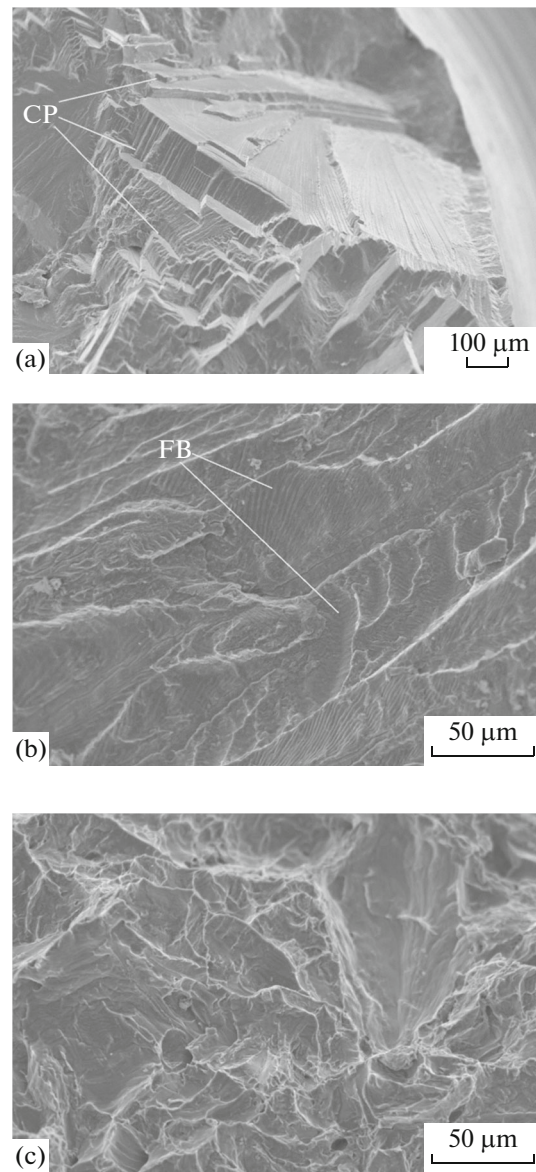


Fig. 9. Fractographic analysis of the fracture surfaces of the CG PT-7M alloy after corrosion–fatigue tests at a stress amplitude of 415 MPa (see Fig. 8c) in zones (a) ZI, (b) ZII, and (c) ZIII. CPs are the crystallographic planes along which cleavage proceeds, and FBs are fatigue beachmarks.

Thus, we can conclude that the RF formation of an UFG structure in the PT-7M alloy increases the fatigue limit by a factor of 1.7–1.8 without changing the fracture mechanism.

The parameters of Basquin's power equation $\sigma_a = AN^{-q}$ were determined by the least squares method for each σ_a – N curve [19]. The numerical values of coefficients A and q are given in Table 1. Interestingly, the dependence of the slope of the σ_a – N fatigue curve on the annealing temperature is nonmonotonic, and UFG structure formation gives rise to an increase in

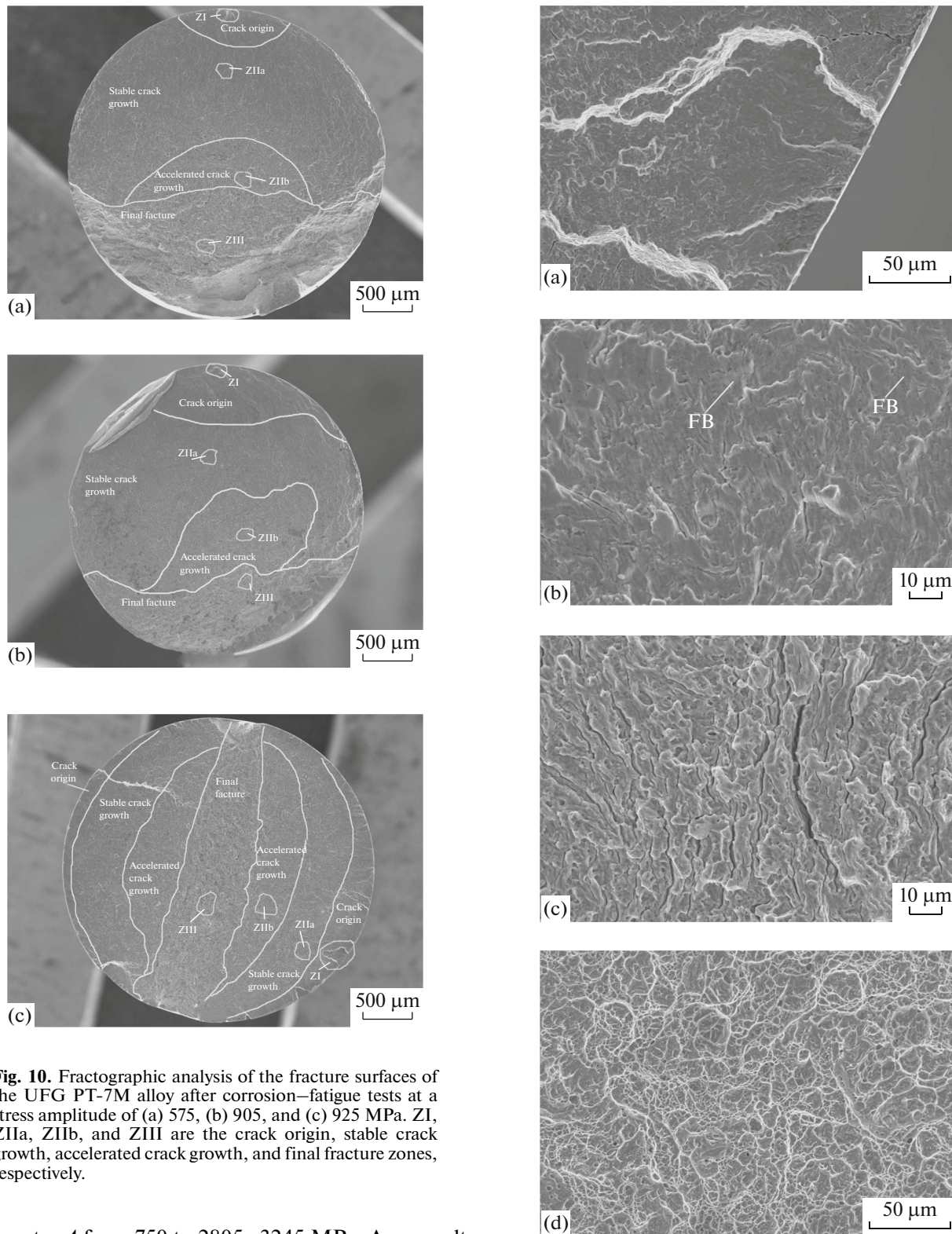


Fig. 10. Fractographic analysis of the fracture surfaces of the UFG PT-7M alloy after corrosion–fatigue tests at a stress amplitude of (a) 575, (b) 905, and (c) 925 MPa. ZI, ZIIa, ZIIb, and ZIII are the crack origin, stable crack growth, accelerated crack growth, and final fracture zones, respectively.

parameter A from 750 to 2805–3245 MPa. As a result of annealing at 500°C, parameter A decreases to 1480 MPa, and the beginning of recrystallization at 550–600°C again increases parameter A to 4810 MPa. After annealing at 650°C, parameter A again decreases to 1570 MPa (see Table 1). This behavior is unexpected, since the slope of the σ_a – N fatigue curve

Fig. 11. Fractographic analysis of the fracture surfaces of the UFG PT-7M alloy after tests at a stress amplitude of 925 MPa (see Fig. 10c) in zones (a) ZI, (b) ZIIa, (c) ZIIb, and (d) ZIII. CP and FB are the same as in Fig. 9.

recorded upon annealing of UFG titanium usually decreases monotonically [23].

The authors of [24, 25] proposed a fatigue fracture model, according to which parameter A is proportional to the free energy of overcoming obstacles by lattice dissociation (ΔF) in the plastic deformation zone in front of a crack tip. (The influence of a corrosive medium on the fatigue fracture of α and pseudo- α titanium alloys is weak because of a high rate of oxide film recovery [17].)

According to [26], ΔF depends substantially on the character of obstacles, namely, the lattice distortion by alloying element atoms, the second-phase particle size, and the dislocation density in a crystal lattice. A change in the type of obstacle that determines the dislocation velocity leads to a change in ΔF and, hence, the slope of the σ_a – N dependence.

The decrease in parameter A after annealing at 400°C can be explained by a decrease in the dislocation density due to recovery. The precipitation of zirconium and α'' -phase particles, which prevent dislocation motion, and the simultaneous formation of internal stress fields at α/α'' interphase boundaries hinder dislocation glide in the grains of the UFG PT-7M titanium alloy and, hence, increase free energy ΔF . The dissolution of zirconium nanoparticles and the intense grain growth during a further increase in the annealing temperature would cause easy dislocation glide in the crystal lattice of α -Ti and, hence, decrease ΔF and the slope of the σ_a – N curve.

The nonmonotonic character of the $A(t)$ can be additionally affected by the complex change in the internal stresses in annealing of the UFG titanium alloy.

As was shown in [4, 27], the dislocation motion in UFG metals depends substantially on long-range internal stress fields, the magnitude of which ($\sigma_{\text{int}} = \alpha_1 \rho_b \Delta b + \alpha_2 w_l$) is proportional to the density of defects in grain boundaries, i.e., misfit dislocations with density $\rho_b \Delta b$ and the gliding components of delocalized dislocations with density w_l (α_1, α_2 are coefficients).

The defect density ($\rho_b \Delta b, w_l$) in grain boundaries depends on the annealing temperature of UFG alloys; during prerecrystallization annealing, the defect density in grain boundaries decreases and, hence, internal stresses σ_{int} also decrease [4, 27].

During recrystallization annealing of the UFG metal, grain boundaries move at velocity V_m and “sweep out” dislocations from its crystal lattice. As a result, a dislocation flux $I = \xi \rho_v V_m$ (ξ is a numerical coefficient, ρ_v is the dislocation density) appears [21, 27, 28], the defect density in the grain boundaries in the UFG alloy increases, and σ_{int} increases. When the annealing temperature increases further, σ_{int} decreases because of an increase in the intensity of diffusion defect recovery in the grain boundaries and a decrease in density ρ_v .

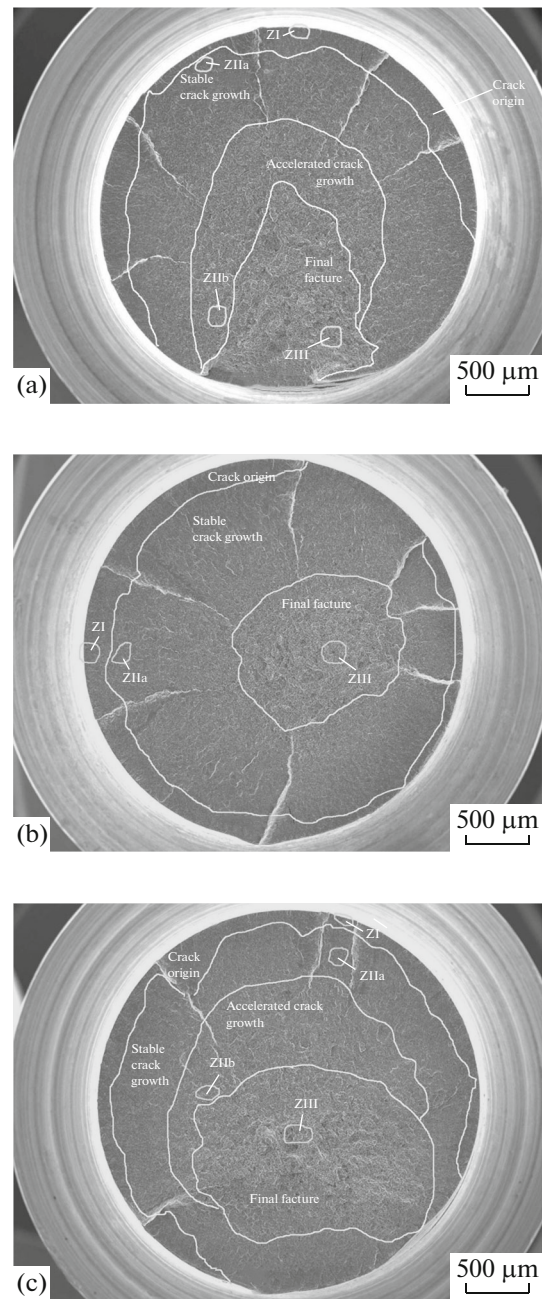


Fig. 12. Fractographic analysis of the fracture surfaces of the UFG PT-7M alloy annealed at 650°C and subjected to corrosion–fatigue tests at a stress amplitude of (a) 615, (b) 730, and (c) 925 MPa. ZI, ZIIa, ZIIb, and ZIII are the same as in Fig. 10.

The nonmonotonic change in σ_{int} on annealing of the UFG alloy is thought to cause a nonmonotonic change in the free energy (ΔF) of overcoming obstacles by lattice dislocations and, hence, a nonmonotonic change in the slope of the σ_a – N fatigue curve on annealing of the UFG PT-7M alloy.

We now discuss the influence of the microstructure parameters on the fatigue crack growth in the UFG titanium alloy.

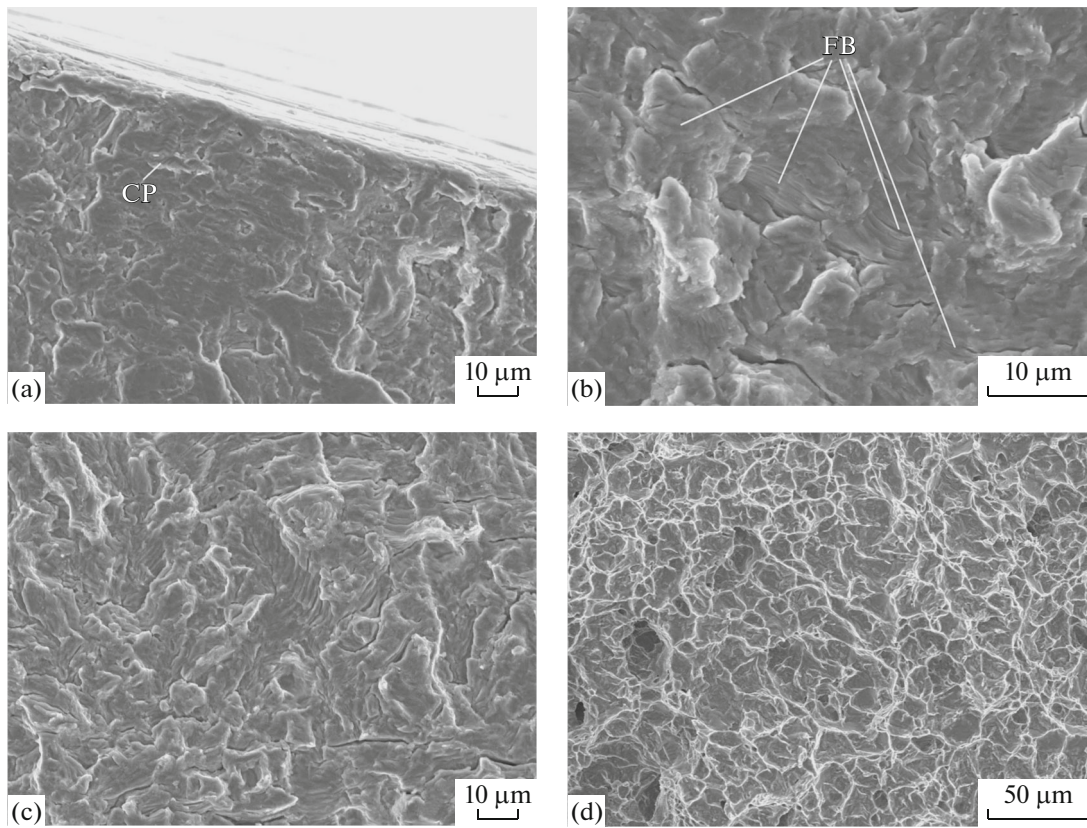


Fig. 13. Fractographic analysis of the fatigue fracture surface of the UFG PT-7M alloy annealed at 650°C and subjected to tests at a stress amplitude of 925 MPa (see Fig. 12c) in zones (a) ZI, (b) ZIIa, (c) ZIIb, and (d) ZIII.

As shown above, the fatigue life of the PT-7M titanium alloy increases after the formation of an UFG structure. Note that fractographic analysis of the fracture surfaces revealed a decrease in the stable crack growth area in the UFG alloy as compared to the CG alloy, and the crack growth rate is known to increase when the grain size decreases [29–33]. In addition, according to XRD data, significant tensile stresses (+520 MPa) appear in the titanium alloy after RF.

Table 1. Constants in Basquin's equation for a PT-7M titanium alloy in various structural states

State of material	Basquin's equation parameters	
	A, MPa	q
Initial	750	0.06
UFG after RF	2805–3245	0.12–0.15
RF + annealing at 500°C for 30 min	1480	0.07
The same at 550°C	4810	0.20
600°C	3545	0.21
650°C	1570	0.10

These stresses decrease the plasticity of the alloy and should accelerate the crack growth and decrease the fatigue life of the titanium alloy.

Our results demonstrate that the crack growth rate in the UFG alloy decreases such that FBs cannot be observed during fractographic examination of the UFG specimens.

This finding is thought to indicate that a factor, which positively affects a decrease in the fatigue crack growth rate, should be operative during fatigue tests of the UFG PT-7M titanium alloy. According to [29–32], this factor in the materials under study under the given experimental conditions can be crack closure. This effect is related to the residual compressive stresses that form in the plasticity zone at the edges of a growing crack, the size of which depends on the applied stress amplitude [29, 33, 34]. The internal stresses in the plasticity zone are rather high and correspond to the yield strength of the material. The negative influence of the internal tensile stresses that appear in the titanium alloy during RF is assumed to be compensated by the formation of compressive stress fields at the tip and edges of a growing fatigue crack.

Thus, the high fatigue characteristics of the UFG PT-7M titanium alloy are assumed to be caused by,

first, a high level of resistance to fatigue crack nucleation, which depends on the density of deformation-induced defects at the nonequilibrium grain boundaries in the UFG alloy, and, second, by the formation of internal stress fields at α/α' interphase boundaries. The difference between the fatigue crack growth rates in the CG and UFG alloys, which manifests itself as a change in the FB–FB distance in the fracture surfaces of the specimens, is less pronounced because of a negative effect of the internal tensile stresses that form during RF and the “compensating” effect of the internal compressive stresses that form at the tip and edges of a growing fatigue crack.

CONCLUSIONS

(1) RF was used to fabricate UFG PT-7M pseudo- α titanium alloy specimens with a high hardness, yield strength, and ultimate tensile strength. The formation of an UFG structure was shown to cause an increase in conventional fatigue limit σ_{-1} (at $N^* = 3 \times 10^6$ cycles) from 320–330 to 570–590 MPa and in fatigue life N_{fr} (at stress amplitude $\sigma_a = 600$ MPa) from 10^3 to 4×10^4 – 5×10^5 loading cycles.

(2) The results of corrosion–fatigue tests of the UFG alloy specimens were found to have a large scatter of experimental points because of a nonuniform strain distribution over the longitudinal section of a titanium rod after RF. As a result, a structure with a higher strength and a smaller grain size forms in the surface layer of a PT-7M titanium alloy rod in comparison with the metal of the central part of the cross section of the rod.

(3) The σ_a – N corrosion fatigue curve of the UFG PT-7M alloy was shown to be described by Basquin’s power equation with a good accuracy. The formation of an UFG structure in the PT-7M alloy was found to increase the slope of the σ_a – N dependence in a low-cycle fatigue range (i.e., to an increase in parameter A in Basquin’s equation ($\sigma_a = AN^{-q}$) from 750 to 2805–3245 MPa). The fracture surfaces of the UFG specimens have a ductile character.

(4) Parameter A in Basquin’s equation for the UFG PT-7M alloy was found to depend on the annealing temperature nonmonotonically (with maximum). The nonmonotonic dependence $A(T_{ann})$ was qualitatively explained. It can be explained by the evolution of the structure of a severely deformed PT-7M alloy in annealing, which results in a decrease in the dislocation density, the precipitation and dissolution of zirconium nanoparticles, the precipitation of α' -phase particles (which induce internal stress fields at α/α' interphase boundaries), and intense grain growth at a high annealing temperature (which increases the defect density at nonequilibrium grain boundaries).

FUNDING

This work was supported by the Russian Science Foundation, project no. 16-13-00066.

REFERENCES

1. I. V. Gorynin and B. B. Chechulin, *Titanium in Mechanical Engineering* (Mashinostroenie, Moscow, 1990).
2. A. S. Oryshchenko, I. V. Gorynin, V. P. Leonov, and I. A. Schastlivaya, “Titanium alloys for low- and medium-power nuclear reactor vessels,” *Vopr. Materialoved.*, No. 2 (78), 199–210 (2014).
3. S. V. Zherebtsov, E. A. Kudryavtsev, G. A. Salishehev, B. B. Straumal, and S. L. Sematin, “Microstructure evolution and mechanical behavior of ultrafine Ti–6Al–4V during low-temperature superplastic deformation,” *Acta Mater.* **121**, 152–163 (2016).
4. V. M. Segal, I. J. Beyerlein, C. N. Tome, V. N. Chuvil’deev, and V. I. Kopylov, *Fundamentals and Engineering of Severe Plastic Deformation* (Nova Sci. Publ., New York, 2010).
5. B. B. Straumal, A. R. Kilmametov, Y. Ivanisenko, A. A. Mazilkin, R. Z. Valiev, N. S. Afonikova, A. S. Gornakova, and H. Hahn, “Diffusive and displacive phase transitions in Ti–Fe and Ti–Co alloys under high pressure torsion,” *J. Alloys Comp.* **735**, 2281–2286 (2018).
6. V. N. Chuvil’deev, V. I. Kopylov, A. M. Bakhmet’ev, N. G. Sandler, A. V. Nokhrin, P. V. Tryaev, Yu. G. Lopatin, N. A. Kozlova, A. V. Piskunov, and N. V. Melekhin, “Effect of a simultaneous increase in the strength and corrosion resistance of microcrystalline titanium alloys,” *Dokl. Akad. Nauk* **442** (3), 329–331 (2012).
7. V. N. Chuvil’deev, V. I. Kopylov, A. V. Nokhrin, A. M. Bakhmet’ev, N. G. Sandler, N. A. Kozlova, P. V. Tryaev, N. Yu. Tabachkova, A. S. Mikhailov, A. V. Ershova, M. Yu. Gryaznov, M. K. Chegurov, A. N. Sysoev, and E. S. Smirnova, “Effect of a simultaneous increase in the strength, plasticity, and corrosion resistance of an ultrafine-grained Ti–4Al–2V pseudo-alpha titanium alloy,” *Pis’ma Zh. Tekh. Fiz.* **43** (10), 25–33 (2017).
8. N. A. Amirkhanova, R. Z. Valiev, E. Yu. Chernyaeva, E. V. Yakushina, and I. P. Semenova, “Corrosion behavior of titanium alloys with an ultrafine-grained structure,” *Russ. Metall. (Metally)*, No. 5, 441–447 (2010).
9. I. P. Semenova, “Strength and high fatigue properties of ultrafine-grained titanium rods produced by severe plastic deformation,” *Russ. Metall. (Metally)*, No. 9, 767–784 (2010).
10. S. V. Zherebtsov, “Efficiency of the strengthening of titanium and titanium alloys of various classes by the formation of an ultrafine-grained structure during severe plastic deformation,” *Russ. Metall. (Metally)*, No. 11, 913–919 (2012).
11. I. V. Gorynin, A. S. Oryshchenko, B. P. Leonov, A. S. Kudryavtsev, V. I. Mikhailov, and E. V. Chudakov, “Marine titanium alloys—present and future,” *Vopr. Materialoved.*, No. 2(78), 36–47 (2014).

12. V. P. Leonov, E. V. Chudakov, and Yu. Yu. Malinkina, "Effect of ruthenium on the structure, corrosion, mechanical properties, and fatigue characteristics of titanium α alloys in a corrosion medium," *Vopr. Materialoved.*, No. 4(88), 106–119 (2016).
13. A. M. Khutyuz, "Fatigue fracture resistance of titanium alloys at a high temperature in a corrosive environment," Extended Abstract of Cand. (Eng.) Sci. Dissertation, Odessa, Odessa Polytechnic Institute, 1992.
14. B. B. Chechulin, S. S. Ushkov, I. N. Razuvaeva, and V. N. Goldfain, *Titanium Alloys in Mechanical Engineering* (Mashinostroenie, Leningrad, 1977).
15. A. G. Illarionov and A. A. Popov, *Technological and Service Properties of Titanium Alloys: Tutorial* (UrFU, Yekaterinburg, 2014).
16. V. I. Pokhmurskii, *Corrosion Fatigue of Metals* (Metallurgiya, Moscow, 1987).
17. H. M. Nykyforchyn, P. Ya. Sydor, O. T. Tsyrunyk, and M. D. Klapkiv, "Influence of hydrogenation of high-temperature corrosion fatigue of α titanium alloys," *Mater. Sci.* **34** (3), 390–397 (1998).
18. G. K. Williamson and W. M. Hall, "X-ray line broadening from field aluminium and wolfram," *Acta Metall.* **1** (1), 22–31 (1953).
19. V. T. Troshchenko and L. A. Sosnovskii, *Fatigue Resistance of Metals and Alloys* (Naukova Dumka, Kiev, 1987).
20. S. S. Gorelik, S. V. Dobatkin, and L. M. Kaputkina, *Recrystallization of Metals and Alloys* (MISIS, Moscow, 2006).
21. A. V. Nokhrin, "Effect of acceleration of grain boundary diffusion during recrystallization in submicrocrystalline metals and alloys formed severe plastic deformation," *Pis'ma Zh. Tekh. Fiz.* **38** (13), 70–78 (2012).
22. J. Fellows, *Fractography and Atlas of Fractograms: A Handbook* (Metallurgiya, Moscow, 1982).
23. A. Yu. Vinogradov, V. V. Stolyarov, S. Hashimoto, and R. Z. Valiev, "Cyclic behavior of ultrafine-grain titanium processed by severe plastic deformation," *Mater. Sci. Eng. A* **318** (1–2), 163–173 (2001).
24. N. N. Berendelev, "Structural model of damage accumulation at the stage of the initiation of a microscopic crack during high-cycle fatigue," Extended Abstract of Cand. (Phys.-Math.) Sci. Dissertation, NNGU, Nizhny Novgorod, 2002.
25. E. N. Butusova, A. V. Nohrin, B. N. Chuvil'deev, D. N. Kotkov, M. S. Boldin, S. P. Stepanov, M. K. Chegurov, N. A. Kozlova, A. S. Mikhailov, and N. N. Viryasova, "Investigation of the nucleation of corrosion fatigue cracks in low-carbon pipe steels," *Vestn. Nizhegorod. Univ.*, No. 5 (2), 177–181 (2010).
26. G. J. Frost and M. F. Ashby, *Deformation Mechanism Maps* (Metallurgiya, Chelyabinsk, 1989).
27. V. N. Chuvil'deev, *Nonequilibrium Grain Boundaries in Metals. Theory and Applications* (Fizmatlit, Moscow, 2004).
28. V. N. Chuvil'deev, A. V. Nokhrin, O. E. Pirozhnikova, M. Yu. Gryaznov, Yu. G. Lopatin, M. M. Myshlyaev, and V. I. Kopylov, "Analysis of changes in the diffusion properties of nonequilibrium grain boundaries during the recrystallization and superplastic deformation of submicrocrystalline metals and alloys," *Fiz. Tverd. Tela* **59** (8), 1561–1569 (2017).
29. S. Suresh, *Fatigue of Materials* (Camb. Univer. Press, Cambridge, 2004).
30. S. Suresh and R. O. Ritchie, "Propagation of short fatigue cracks," *Int. Met. Rev.* **29** (6), 445–475 (1984).
31. R. Pippan and A. Honenwarter, "Fatigue crack closure: a review of the physical phenomena," *Fatig. Fract. Eng. Mater. Struct.* **40**, 471–495 (2017).
32. R. Pippan and F. O. Riemelmoser, "Modeling of fatigue crack growth: dislocation models," *Compreh. Struct. Integr.* **4**, 191–207 (2003).
33. K. J. Miller, "The short crack problem," *Fatig. Fract. Eng. Mater. Struct.* **5** (3), 223–232 (1982).
34. T. Vojtek, R. Pippan, A. Hohenwarter, and J. Porluda, "Prediction of effective mode II fatigue crack growth threshold for metallic materials," *Eng. Fract. Meehan.* **174**, 117–126 (2017).

Translated by K. Shakhlevich